

Microstructure characterization, phase transition, and device application of phase-change memory materials

Kai Jiang ^{a,b}, Shubing Li^b, Fangfang Chen^a, Liping Zhu^c and Wenwu Li ^{b,d}

^aSchool of Arts and Sciences, Shanghai Dianji University, Shanghai, China;

^bDepartment of Physics, East China Normal University, Shanghai, China;

^cState Key Laboratory of Surface Physics and Institute for Nanoelectronic Devices and Quantum Computing, Department of Physics, Fudan University, Shanghai, China;

^dShanghai Frontiers Science Research Base of Intelligent Optoelectronics and Perception, Institute of Optoelectronics, Department of Materials Science, Fudan University, Shanghai, China

ABSTRACT

Phase-change memory (PCM), recently developed as the storage-class memory in a computer system, is a new non-volatile memory technology. In addition, the applications of PCM in a non-von Neumann computing, such as neuromorphic computing and in-memory computing, are being investigated. Although PCM-based devices have been extensively studied, several concerns regarding the electrical, thermal, and structural dynamics of phase-change devices remain. In this article, aiming at PCM devices, a comprehensive review of PCM materials is provided, including the primary PCM device mechanics that underpin read and write operations, physics-based modeling initiatives and experimental characterization of the many features examined in nanoscale PCM devices. Finally, this review will propose a prognosis on a few unsolved challenges and highlight research areas of further investigation.

ARTICLE HISTORY

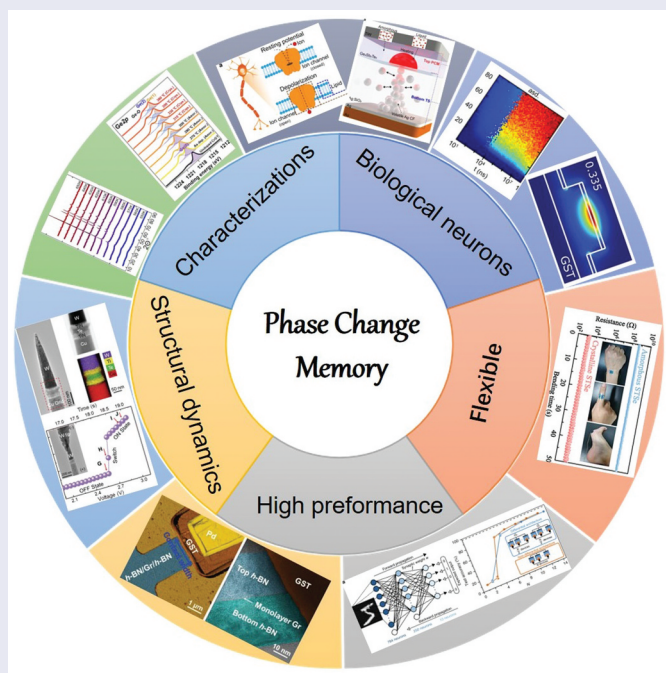
Received 30 March 2023

Revised 10 July 2023

Accepted 23 August 2023

KEYWORDS

Phase-change memory; structural regulation; in-situ characterization; flexible devices



IMPACT STATEMENT

We certify that the submitted manuscript is truly original, unpublished, and not being considered for publication elsewhere.

Introduction

Recently, the demand for data storage has exponentially increased and attracted considerable attention compared

with other memory technologies. Since the development of data storage technologies, several memory

CONTACT Fangfang Chen  chenff@sdju.edu.cn  School of Arts and Sciences, Shanghai Dianji University, Shanghai 200240, China; Liping Zhu  zhuliping@fudan.edu.cn  State Key Laboratory of Surface Physics and Institute for Nanoelectronic Devices and Quantum Computing, Department of Physics, Fudan University, Shanghai 200433, China; Wenwu Li  liwenwu@fudan.edu.cn  Shanghai Frontiers Science Research Base of Intelligent Optoelectronics and Perception, Institute of Optoelectronics, Department of Materials Science, Fudan University, Shanghai, China

© 2023 The Author(s). Published by National Institute for Materials Science in partnership with Taylor & Francis Group.

This is an Open Access article distributed under the terms of the Creative Commons Attribution-NonCommercial License (<http://creativecommons.org/licenses/by-nc/4.0/>), which permits unrestricted non-commercial use, distribution, and reproduction in any medium, provided the original work is properly cited. The terms on which this article has been published allow the posting of the Accepted Manuscript in a repository by the author(s) or with their consent.

technologies have emerged, providing diverse choices for the next generation of storage [1–5]. To improve data-computing efficiency and energy utilization, a series of universal memory data storage devices with advantages, such as low power consumption and moderate price of dynamic random-access memory (DRAM) and high operating speeds of static random-access memory (SRAM) was proposed [6–12]. However, SRAM and DRAM are volatile, and data is lost after a power outage. Conversely, non-volatile memory can store data for tens of years in the power-off state and thus has been attracting increasing research attention. The fast and non-volatile properties can bridge the memory wall between the volatile DRAM and the non-volatile solid-state disk. The resistance random-access memory is a promising candidate for high-density storage owing to its simple crossbar structure [9,13]. Commercialized magnetic random-access memory (MRAM) is advantageous for its low power and high-speed consumption. As non-volatile memory, the high-performance and high-scalability phase-change random-access memory (PCRAM) can operate in the order of nanoseconds and has been a leading candidate among the emerging nonvolatile memory technologies for next-generation electronic devices [14–16]. In PCRAM, phase change materials are the core components, so in-depth research on the microstructure characterization and device applications of phase-change materials is of great significance.

Phase change materials are the core materials of phase change memory, and the research and development of phase change materials directly affect the performance and application of phase change memory. Therefore, the research and development of phase change materials is an important foundation for the

development of phase change memory. Data storage in PCRAM is realized by the large electrical and optical properties of its crystalline and amorphous states in chalcogenide materials. In general, the flagship phase change material is ternary $\text{Ge}_2\text{Sb}_2\text{Te}_5$, which is a pseudo-binary chalcogenide material typically comprising Sb_2Te_3 and GeTe [17–22]. In amorphous Ge–Sb–Te (GST) compounds, the atoms are randomly distributed without long-range order and can be sequentially crystallized into an equilibrium hexagonal structure, as illustrated in Figure 1(a) [23]. The crystalline states generally exhibit low electrical resistivity and low transmittance, whereas the amorphous states exhibit high electrical resistivity and high transmittance. The crystalline state exhibits electricity two to six orders of magnitude lower than that of the amorphous state, and the two states can be reversibly switched by current pulses or light pulses at different durations and intensities. The PCM can be crystallized from the amorphous under the application of a long low current pulse (above crystalline temperature T_c , below melting point T_m) for the SET/write operation at a temperature of ~ 500 K; and recrystallized from the crystalline state under the application of a short high current pulse (above T_c) for the RESET/erase operation at a temperature > 1000 K, as shown in Figure 1(b) [24]. The crystallization speed is tens to hundreds of nanoseconds, while the amorphization process can be as fast as hundreds of picoseconds.

The PCM acts as a core layer in commercialized PCRAM and plays an important role. The first chalcogenide PCM, GeSiAsTe , was originally proposed by Ovshinsky et al. in 1968, and the GST compounds were subsequently discovered. Following these

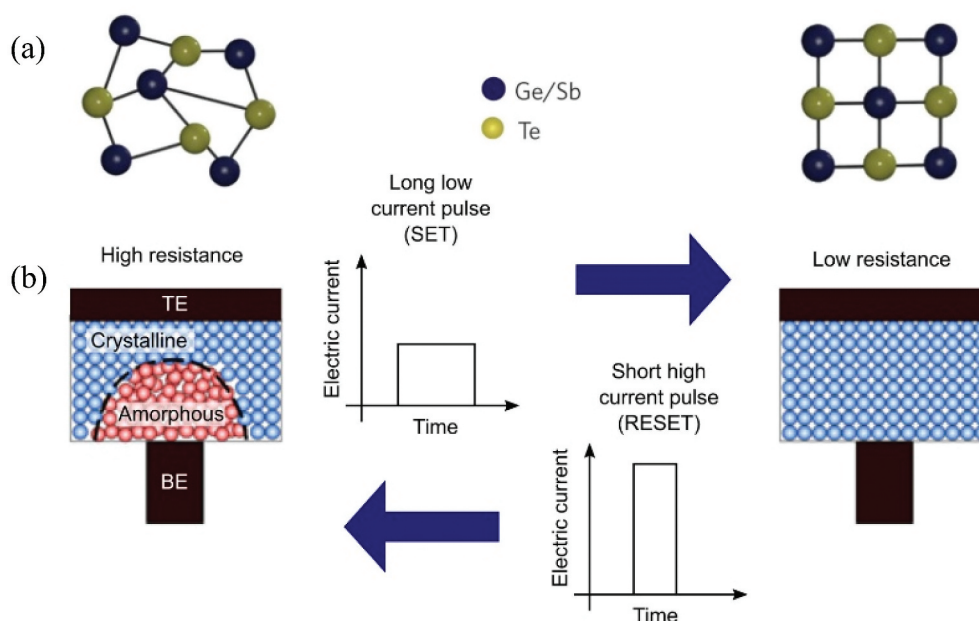


Figure 1. (a) Crystal structures of amorphous and crystalline $\text{Ge}_2\text{Sb}_2\text{Te}_5$ (GST). Reproduced by permission from [23], copyright [2015, Springer] (b) Diagram of operation principle in PCM. Reproduced by permission from [24], copyright [2020, IOP].

pioneering reports, in the GST alloys, $\text{Ag}_5\text{In}_5\text{Sb}_{60}\text{Te}_{30}$ and $\text{Ag}_4\text{In}_2\text{Sb}_{67}\text{Te}_{26}$ were found to exhibit fast crystallization and favorable optical reflectivity contrast, facilitating their wide application in rewritable optical storage products, such as digital versatile disks (DVD)-RAM, DVD-rewritable disks, and Blu-ray discs. With the development of material science, PCMs are increasingly being discovered and more detailed phase diagrams are being developed. Until now, Te-containing chalcogenide PCMs have been significantly studied, but few non-chalcogenide alloys and elementary substances have. The crystallization mechanisms of PCMs can be broadly divided into nucleation-driven and growth-driven types, according to the crystallization kinetics. For the nucleation-driven type PCMs, such as Sb_2Te_3 , crystallization occurs via the formation of critical nuclei and subsequent growth, exhibiting fast nucleation. In contrast, the crystallization of those growth-driven PCMs occurs in the amorphous region surrounded by a crystalline matrix; it rapidly proceeds, and no sizeable nor robust crystalline seeds form during the short timescale involved in the growth process. Moreover, doping engineering, including W-doped $\text{Ge}_2\text{Sb}_2\text{Te}_5$, Sc-

doped Sb_2Te_3 , and Se-doped GeTe , is frequently used to improve the intrinsic properties of PCM, providing different material characteristics to consequently meet the requirements in different scenarios.

In this review, we outline the recent advancements in the characterization of PCM and device performances, including physical characteristics, crystallization dynamics, structural design, and storage performance. Moreover, we anticipate further advancements in PCM technology.

Recent progress in PCM

The rate at which the materials crystallize essentially restricts the performance of RAM devices that depend on phase shifts. For the sake of achieve high speed PCRAM, the materials design needs to identify and transition metals are good dopants choice. To fabricate scandium-doped antimony telluride with a subnanosecond crystallization speed, Rao et al. integrated the theory with a straightforward set of selection criteria [25]. As shown in Figure 2(a), using initial theoretical calculations and molecular dynamics simulations, scandium, a transition group element,

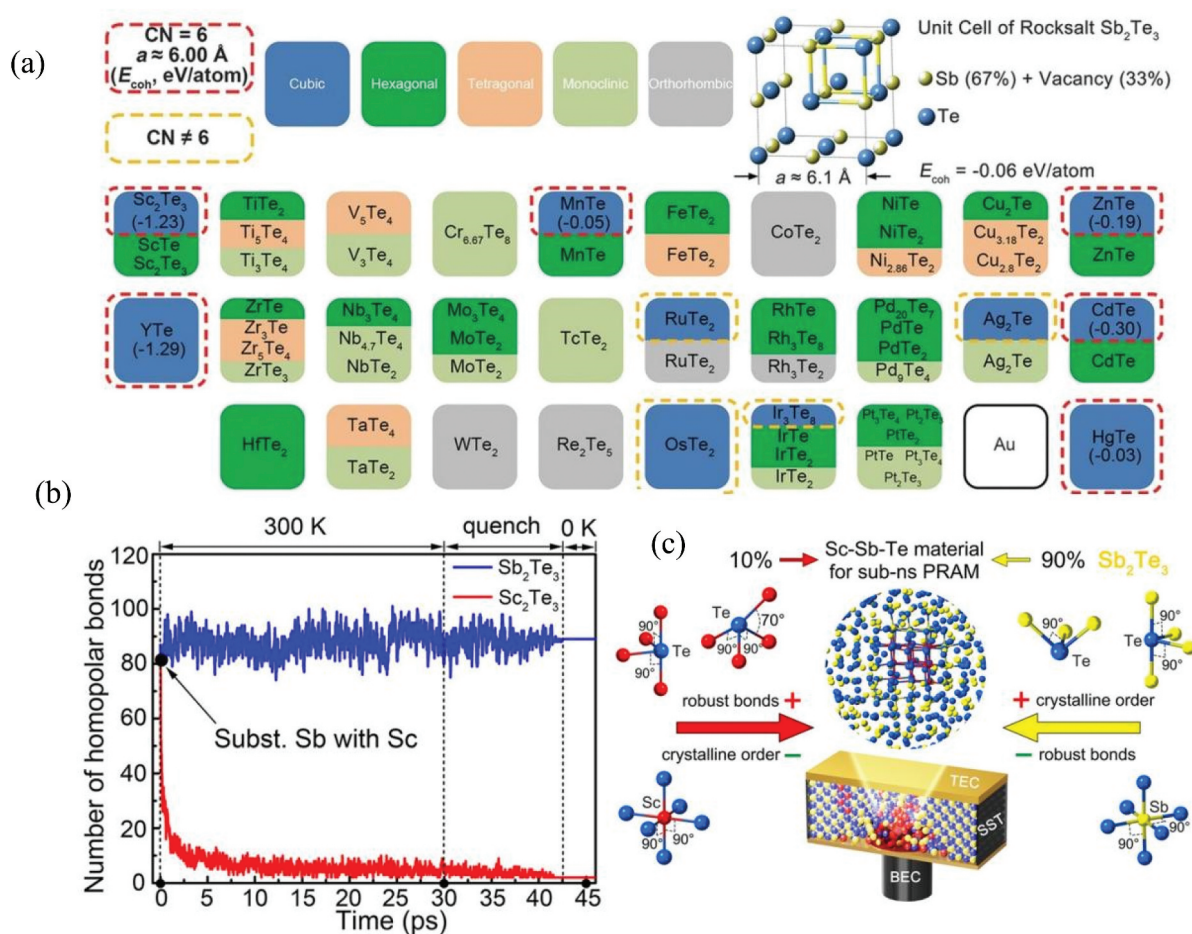


Figure 2. (a) Screening geometrically matched transition metal (TM) tellurides with high-strength TM–Te bonds for rock-salt Sb_2Te_3 . Reproduced by permission from [25], copyright [2017, AAAS] (b) Strong relaxation of a- Sc_2Te_3 in the presence of homopolar bonds. (c) Chemical design principles for cache-type Sc-Sb-Te compounds. Reproduced by permission from [26], copyright [2019, ACS].

was used as the doping element. They created a scandium-doped antimony telluride (SST) material with excellent stability, extended life, and low power consumption. To accomplish a high-speed reversible write – erase operation of 700 ps, the researchers employed the SST-based PCRAM fabricated using the complementary metal-oxide-semiconductor technique. It approaches the upper bound of the existing PCRAM, which is already comparable to the crucial conversion effect’s resistance conversion speed. The number of cycles is $>10^7$. SST-based PCRAM power consumption is 90% less than those of conventional GST devices. The comprehensive performance of SST-based PCRAM is further enhanced, facilitating the creation of general-purpose memory by further optimizing the material and minimizing the device size. Improved crystal nucleation in Sc–Sb–Te PCMs has helped realized sub-nanosecond switching in PCM devices. It is crucial to determine a method to modify the chemical makeup of scandium antimony tellurium to optimize device performance. First-principles simulations and quantum chemical bond analysis for the pertinent parent compounds of the SST alloy, Sc_2Te_3 and Sb_2Te_3 , were conducted. Zewdie et al. discovered that the amorphous phases had comparable bond lengths and angles [26]. Figure 2(b) shows the strong relaxation of a- Sc_2Te_3 in the presence of homopolar bonds. The lack of homopolar bonds in Sc_2O_3 arises from the strong charge transfer and the ensuing high energy cost. When 10% scandium telluride and 90% antimony telluride are fused to create scandium

antimony tellurium alloy, the stable scandium tellurium tetra ternary ring can significantly increase the crystallization efficiency of the system as shown in Figure 2(c), optimizing the operating speed of the scandium antimony tellurium phase change device. The robustness of Sc–Te bonds explains the enhanced nucleation in Sc–Sb–Te compounds, thereby enabling subnanosecond memory operations.

The development and design of conductive bridge low-power PCM material are powerful tools to maximize memory performance. A type of PCM with a mesh amorphous structure with a power consumption of < 0.05 pJ, which is 1000 times lower than those of conventional products, was fabricated by Yang et al. ‘Nano-bridges’ that connect the crystalline domains into a conductive channel (Figure 3(a)) were created and fractured to constrain the following phase-change switching in the region where the crystalline nanodomain meets its amorphous surrounding [27]. The new PCM/fabrication is completely compatible with the existing 3D integration technology and does not require any additional costs or processing. The memory cell exhibits favorable cycling performance, as shown in Figure 3(b). These GST alloy materials rapidly crystallize into rock salt-like phases with significant structural and vacancy disorders and transition into an insulating phase at low temperatures. Xu et. al. comprehensively described the crystallization dynamics and physical properties of $GeSb_2Te_4$ using first-principles calculations based on quantum mechanics [28]. Figure 3(c) shows the crystallization

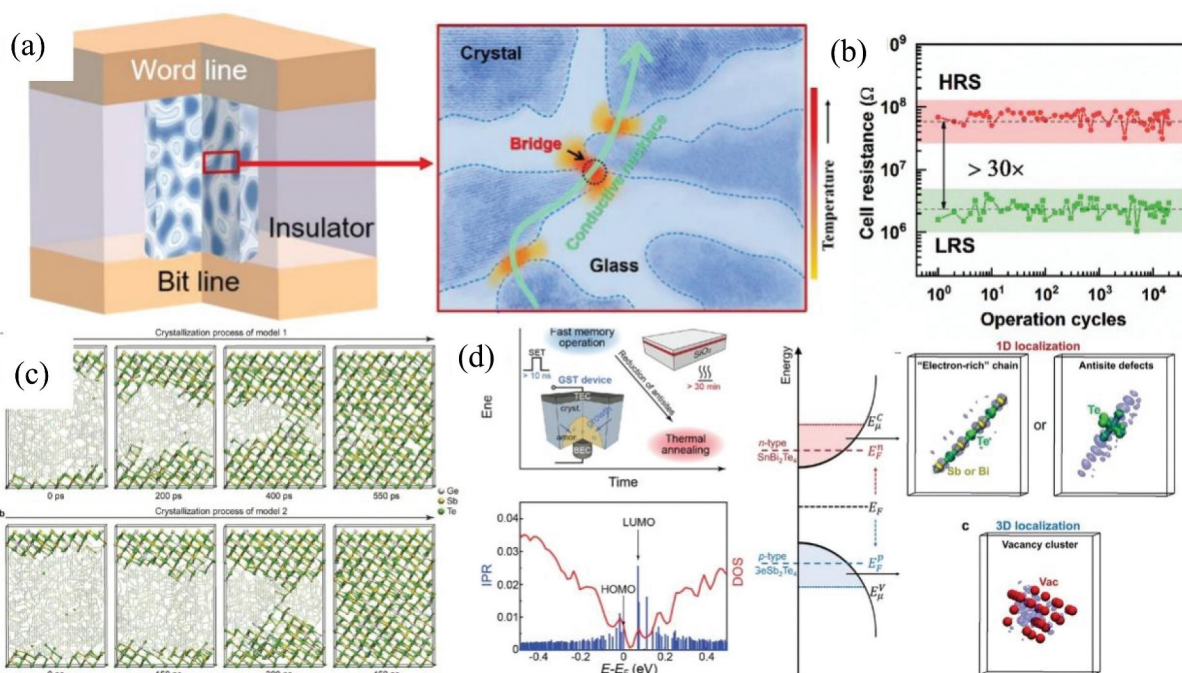


Figure 3. (a) Concept of conductive-bridge phase-change memory. (b) Cycling programming for one typical memory cell. HRS and LRS stand for high-resistance state and low-resistance state. Reproduced by permission from [27], copyright [2022, Wiley] (c) Simulated crystallization of a 1008-atom model of $GeSb_2Te_4$ PCM. (d) Band structure of PCM. Reproduced by permission from [28], copyright [2022, Wiley].

dynamics of the GeSb_2Te_4 PCM. The transport properties of GST are examined concerning the relationship between the electronic and structural properties. In addition, Figure 3(d) shows the electronic band structure which can be facilitated by extended Sb-rich motifs and antisite defects. Such instruments for structural characterization would not only serve as a useful example to develop heterogeneous PCMs, but also minimizing the active switching volume for low-power electronics, which will attract more attention in the future.

PCMs are crucial for computer memory because they can store data by changing their physical state, such as sing a thermal pulse, they can swiftly change from glassy to crystalline and retain that form for long periods at lower temperatures. For many years, the structures of some PCMs in the amorphous phase were under debate. Although their employment in memory technology is enabled by the temperature-dependent kinetics of their crystallization process, the transition on an atomic level is yet to be understood. Zalden et al. examined the underlying atomic structure of two PCMs during this shift using ultrafast X-rays and simulations [29]. Figure 4(a) shows the relationship between the structural parameter $R = r_2/r_1$, pre-peak intensity, and apparent activation energy of diffusivity as a function of temperature. Without interference from crystallization, ultrafast X-ray diffraction following short-pulse stimulation provides access to the atomic structure of PCMs

during the entire melt-quench cycle. The liquid – liquid phase transition at 660 and 610 K were observed in the PCMs $\text{Ag}_4\text{In}_3\text{Sb}_{67}\text{Te}_{26}$ and $\text{Ge}_{15}\text{Sb}_{85}$, respectively. X-ray diffraction patterns was used by Xu et al. to investigate the metal-insulator transition and the phase change induced by Se doping in $\text{Ge}_2\text{Sb}_2\text{Se}_{5x}\text{Te}_{5-x}$ [30]. As shown in Figure 4(b,c), when amorphous $\text{Ge}_2\text{Sb}_2\text{Se}_{4.5}\text{Te}_{0.5}$ is heated to 650 K from room temperature, partial crystallization is observed at 580 K. According to the isothermal differential scanning calorimetry (DSC) measurements of the crystallization activation energy, the amorphous state is reasonably stable. The initiation of Peierls distortions is the primary cause of the changeover. Shuang et al. used X-ray absorption near edge structure and hard X-ray photoelectron spectroscopy to investigate the local structure surrounding the nitrogen dopant in the phase transition material $\text{Cr}_2\text{Ge}_2\text{Te}_6$ [31]. Figure 4(d,e) show the spectra of nitrogen-doped $\text{Cr}_2\text{Ge}_2\text{Te}_6$ films as a function of annealing temperature. The development of Cr nanoclusters in the amorphous nitrogen-doped $\text{Cr}_2\text{Ge}_2\text{Te}_6$ phase is inhibited by the nitrogen doping. The aforementioned structure analysis of PCMs play an essential role in achieving high-speed phase change memory.

The crystallization tendencies of PCMs are essential for neuromorphic and non-volatile memory applications. Cheng et al. reported a theoretically novel method to control the PCM crystallization based on modifying the β -relaxations and demonstrated that

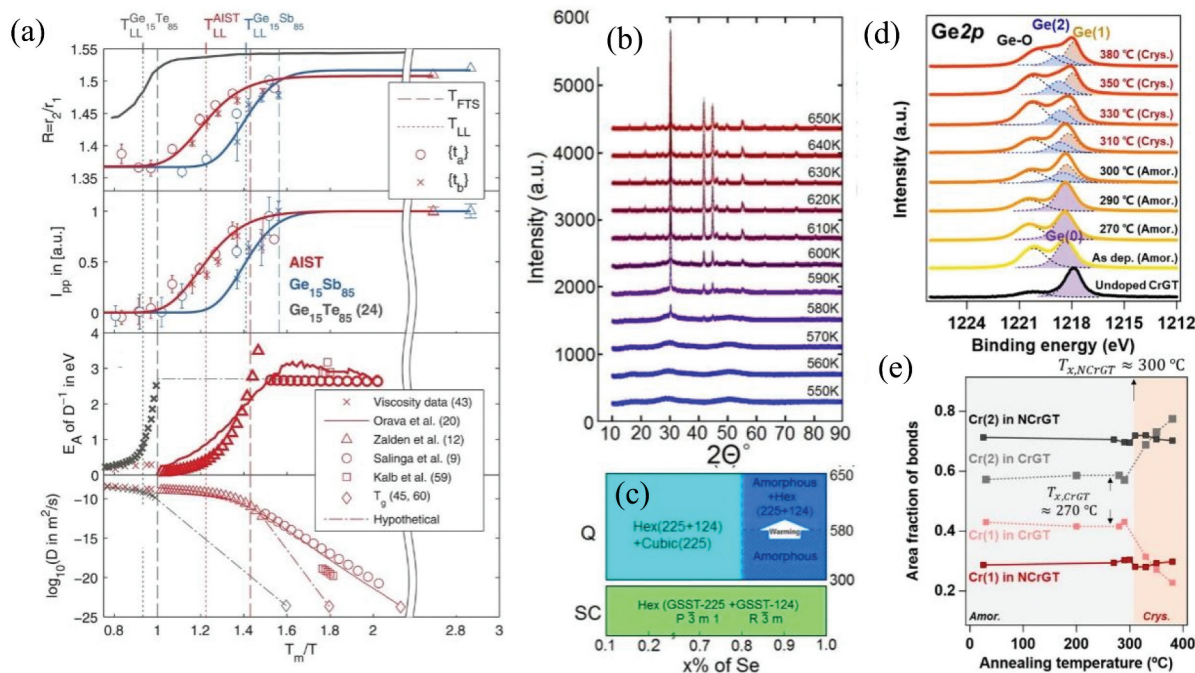


Figure 4. (a) The structural parameter, the intensity of a pre-peak, and apparent activation energy diffusivity as a function of temperature for $\text{Ag}_4\text{In}_3\text{Sb}_{67}\text{Te}_{26}$. Reproduced by permission from [29], copyright [2019, AAAS] (b) Evolution of the diffraction pattern as a function of temperature. (c) Schematic phase diagram summarizing the results of the $\text{Ge}_2\text{Sb}_2\text{Se}_{5x}\text{Te}_{5-x}$ system. Reproduced by permission from [30], copyright [2020, AIP] (d, e) X-ray photoelectron spectroscopy (XPS) profiles and peak area fractions of the films as a function of temperature. Reproduced by permission from [31], copyright [2021, Elsevier].

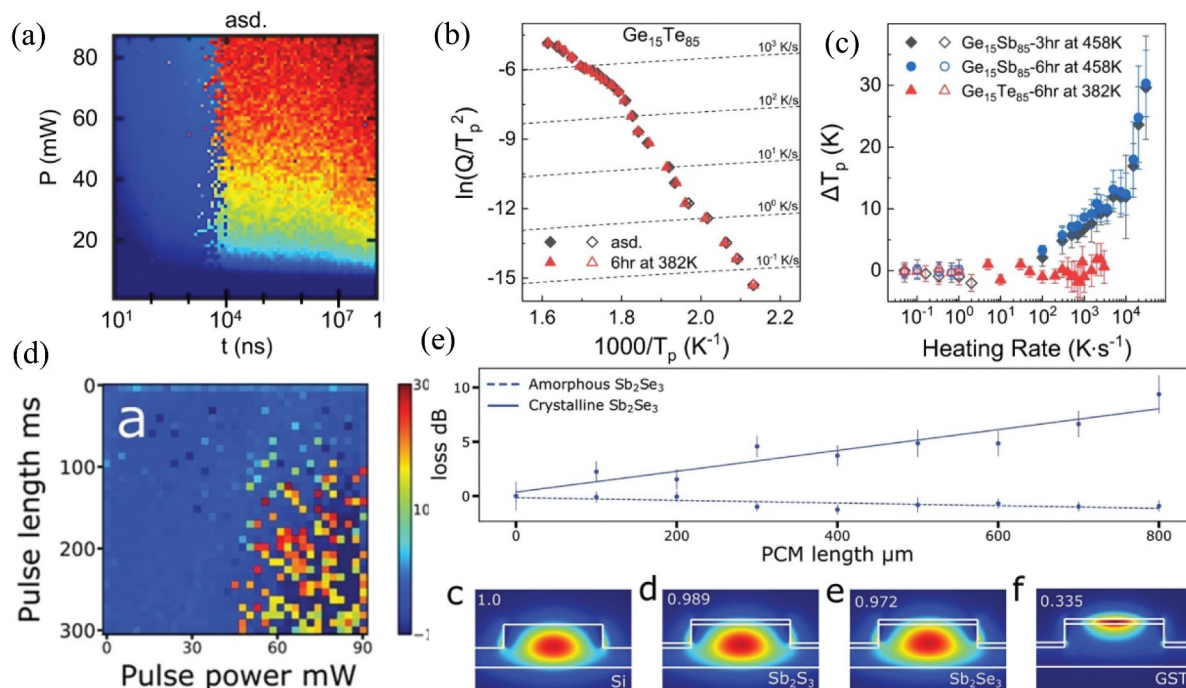


Figure 5. (a) Crystallization time as a function of laser pulse duration. (b, c) crystallization and temperature of the principal crystallization peak (T_p) for as-deposited and annealed samples, respectively. Reproduced by permission from [32], copyright [2022, Springer] (d) Change in reflection as a function of crystallization pulse parameters. (e) Loss in dB for different lengths of Sb_2Se_3 cladding in both amorphous and crystalline phases. Reproduced by permission from [33], copyright [2020, Wiley].

crystallization and β -relaxations are closely related [32]. They discovered that the remarkable tunability of β -relaxations in $Ge_{15}Sb_{85}$ allows them to control the crystallization kinetics by an order of magnitude. According to the in-situ synchrotron X-ray scattering results, dielectric functions, and first principles calculations, as shown in Figure 5(a–c), the local reinforcement distortions cause the decrease in relaxation intensity. Delaney et al. experimentally demonstrated that Sb_2S_3 and Sb_2Se_3 are a new family of ultralow loss reversible phase-change materials for photonic integrated circuits [33]. Raman spectroscopy and optical microscopy were used to validate the phase transition, and X-ray photoelectron spectroscopy (XPS) and ellipsometry were used to assess the composition and refractive index of the optimized films. In both amorphous and crystalline phases, the real parts of the refractive index are significantly more closely matched to that of silicon than GST; this helps with mode matching in integrated device configurations. As we know, the crystallization process is a thermodynamic mechanism, which requires the material to be cooled from above its crystallization temperature. Figure 5(d) show the levels of crystallization with pulses of varying length and energy. We can find a minimum pulse power of 45 mW and a pulse duration of 100 ms are required to achieve any crystallization. The switching characteristics of the phase-change materials are of extreme interest for applications in integrated photonics, and particularly for silicon photonics. When integrating these materials into a common silicon

photonics platform, a new figure of merit (FOM) is established to account for the observed waveguide losses to overcome the almost negligible inherent absorption losses. As shown in Figure 5(e), the Sb_2S_3 and Sb_2Se_3 materials presented a propagation loss that is two orders of magnitudes lower than the commonly used GST. The use of these new phase-change materials will provide a step change in scalable, low cost, and fully programmable optical processing units compatible with the silicon photonics platform. Beyond the use in silicon photonics, these low-loss phase-change materials will find use in high quality nanophotonic resonators and tunable plasmonic nanodevices. This provides a new family of ultralow loss reversible phase change materials for photonic integrated circuits a new insight into on-chip programmable phase control, which would open novel directions in programmable integrated photonic circuits and nanophotonic devices.

Information can be stored and processed via PCRAM. In addition, noise and electrical drifts are problems because of damage accumulation from the cycling process. Ding et al. created a phase-change heterostructure (PCH) comprising alternatively stacked PCM and confinement material [34]. Among them, the spatial limitation layer between the PCM layers may prevent the component and structural changes that occur during the phase change storage cycle, thus minimizing noise and resistance drift and enabling stable and quicker storage, as shown in Figure 6(a). Figure 6(b) shows the improved RESET

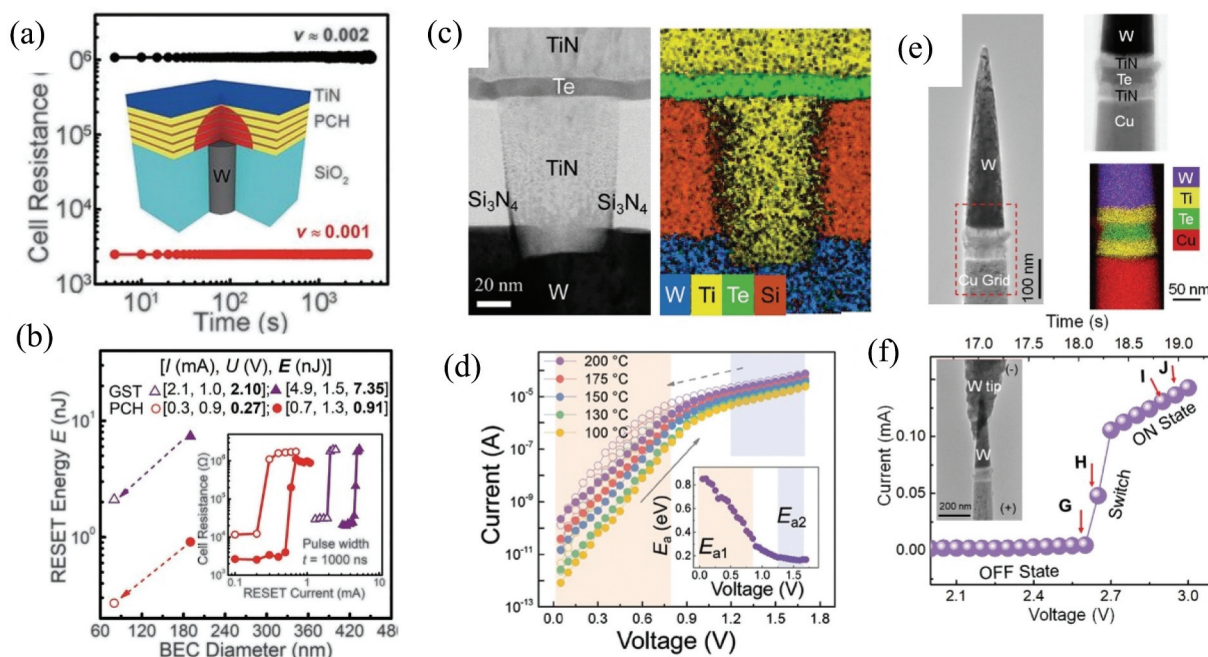


Figure 6. (a) Suppressed resistance drift: cell resistance as a function of time for the RESET and SET state of the PCH device. (b) Improved RESET energy as a function of bottom electrode contact diameter for GST and PCH devices. Reproduced by permission from [34], copyright [2019, AAAS] (c) Cross-sectional TEM image of a Te cell. (d) I - V characteristics of a Te switch with different temperatures. (e) TEM image of a TiN/Te/TiN nanodevice. (f) DC I - V curve of the Te nanodevice during switching. Reproduced by permission from [35], copyright [2021, AAAS].

energy as a function of bottom electrode contact diameter for the GST and PCH devices. Notably, during the repetitive RESET operation, the PCH-based PCRAM device can provide nine stable polymorphic storage (the resistance drift coefficient of each resistance state is < 0.005 , significantly lower than the resistance drift value of 0.11 of the amorphous GST device). During the cumulative SET operation, the device conductance remains consistent (fluctuation $< 9\%$, whereas GST device fluctuation is $> 40\%$). Additionally, PCH devices have operation speeds that are one order of magnitude higher (up to 10 ns), an operation life that is three orders of magnitude longer (PCH device cycle life is approximately 10^9 , whereas that of GST devices is 10^6), and an operation power consumption that over 87% lower than those of GST-based devices. The PCH architecture and the method of alternate stacking of functional nanolayers is amenable to industrial production and easily incorporated into state-of-the-art device setups for applications, which demonstrate bright application prospects.

PCMs comprise switches and storage components. Shen et al. reported that single-element electrical switches may increase the compactness of memory chips [35]. As shown in Figure 6(c), a Te volatile switch with a switching speed of < 20 ns and a significant driving current density is proposed (Figure 6(d)). The I - V curve is shown in Figure 6(f). The 0.95 eV Schottky barrier at the interface causes the low OFF current, and the melting of the crystal liquid generated by the transient voltage pulse of pure Te

brings on the large ON current. The discovery of the Te single-element electrical switch by Shen et al. helps realize denser memory chips and provides a new perspective for 3D XPoint architectures.

Owing to its exceptional thermal stability and extremely high cycle durability, C-doped Ge₂Sb₂Te₅ (CGST) is a potential candidate for PCRAM. Cheng et al. used spherical aberration-corrected transmission electron microscopy to establish the influence of C-dopant on the mechanism of microstructure development [36]. Figure 7(a,b) show the high-angle dark field scanning transmission electron microscopy (HAADF-STEM) image and cell cyclability, respectively. Current pulse stimulation ruptures the C - Ge bond, subsequently causing the assembling of stochastic grain-outer C clusters in the active area; this effectively suppresses grain growth and elemental segregation to increase device reliability. The performance of the device can be affected by differences in C doping, and this has wide implications for improving the microstructure transition and achieving the C-doped material system. Based on a meticulous experimental plan to manufacture a series of Y_xSb_{2-x}Te₃ (YST, $0 \leq x \leq 0.333$) PCMs, Liu et al. showed that Y_{0.25}Sb_{1.75}Te₃ is an ideal candidate material [37]. As shown in Figure 7(c,d), the reversible multi-level phase transitions between three states (amorphous, metastable cubic, and stable hexagonal crystalline phases) are used in novel multi-level data storage systems with yttrium-doped antimony telluride. The apparent reversible cubic-to-hexagonal transition is attributable to the sequential and directed movement

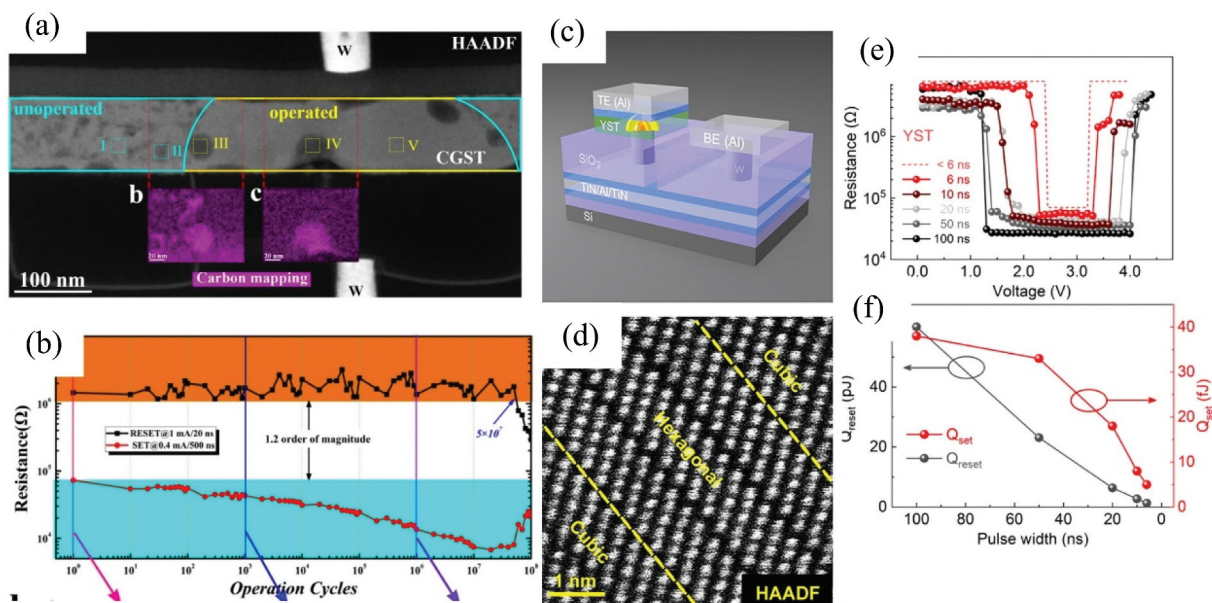


Figure 7. (a) Elemental variations in the CGST film after cyclic failure. (b) Typical cell cyclability of CGST-based PCRAM device. Reproduced by permission from [36], copyright [2020, ACS] (c) Schematic of a T-shaped PCM cell (d) HAADF-STEM image of intermediate state during metastabilization. Reproduced by permission from [37], copyright [2021, Elsevier] (e) Resistance-voltage curves of $Y_{0.25}Sb_{1.75}Te_3$ (YST)-based PCRAM device. (f) Calculated power consumption for the set and reset processes. Reproduced by permission from [38], copyright [2020, ACS].

of Sb atoms, whereas the metastable cubic phase is supported by yttrium. Figure 7(e,f) show the resistance – voltage curves and the power consumption for the set and reset processes, respectively [38]. Even when integrated into a standard T-shaped device, the YST PCM displays a considerably low reset power consumption of 1.3 pJ and a competitively high set speed of 6 ns. The low power consumption is ascribable to the reduced thermal and electrical conductivities, whereas the competitively high crystallization speed is attributable to the preserved crystal structure of Sb_2Te_3 and grain refining. The work proved a new YST-based PCMs by doping engineering with lower power consumption and fast speed, which is a good candidate for universal memory.

As heating electrodes for PCM, graphene nanoribbons (GNRs) are quasi-one-dimensional graphene nanostructures with extremely high current-carrying capacity ($>10^9$ A/cm²) and favorable thermal stability. Wang et al. fabricated a high-performance compact phase-change storage cell using GNR edge contacts [13]. The device size helps achieve low power consumption, high programming speed, high/low resistance ratio, and excellent stability/durability. As shown in Figure 8(a,b), the scaling limit of phase-change storage technology is almost reached. In a cell with a 3 nm-wide GNR as the edge contact and 1 nm² cross-sectional area, the power consumption may be lowered to 53.7 fJ. Figure 8(c–e) illustrate the high performance of the memory cell. It is observed that the polarity of the bias pulse controls the duration of a cycle in the asymmetric structure. The endurance can be increased by at least one order of magnitude by

providing a positive bias to the graphene electrode rather than when the polarity is reversed. This innovation provides valuable insights into the PCRAM technology and its potential applications for future in-memory computing.

PCMs are appealing for computer memory and processing applications because they convert structural changes into variations in electrical resistance. Owing to its dependability, compatibility, and high performance, flexible memory and wearable electronics constitute an emerging technology. Khan et al. directly deposited layers of antimony telluride and germanium telluride on a flexible polyimide substrate and created a flexible PCM device [40]. A schematic of the device and optical images of fabricated devices are shown in Figure 9(a). Flexible superlattice PCM shown in Figure 9(b) has a switching current density of 10^6 A/cm². The gadget operates on several levels using little switching current density. The low switching current and excellent on/off resistance ratio are maintained. Li et al. built a flexible electrical device using aluminum alloy sheets and silver adhesives for fastening after bending [41]. Under various bending states, as shown in Figure 9(c), the switching ratios of the flexible devices are retained at six orders of magnitude. Figure 9(d) shows a schematic of the flexible device structure. Moreover, Li et al. reported improved thermal stability in the $Sb_2Te_xSe_{3-x}$ (STSe) PCM for applications as well as wearable electronics [42]. As shown in Figure 9(e,f), the STSe device has an exceptional endurance of over 100 s and a longer

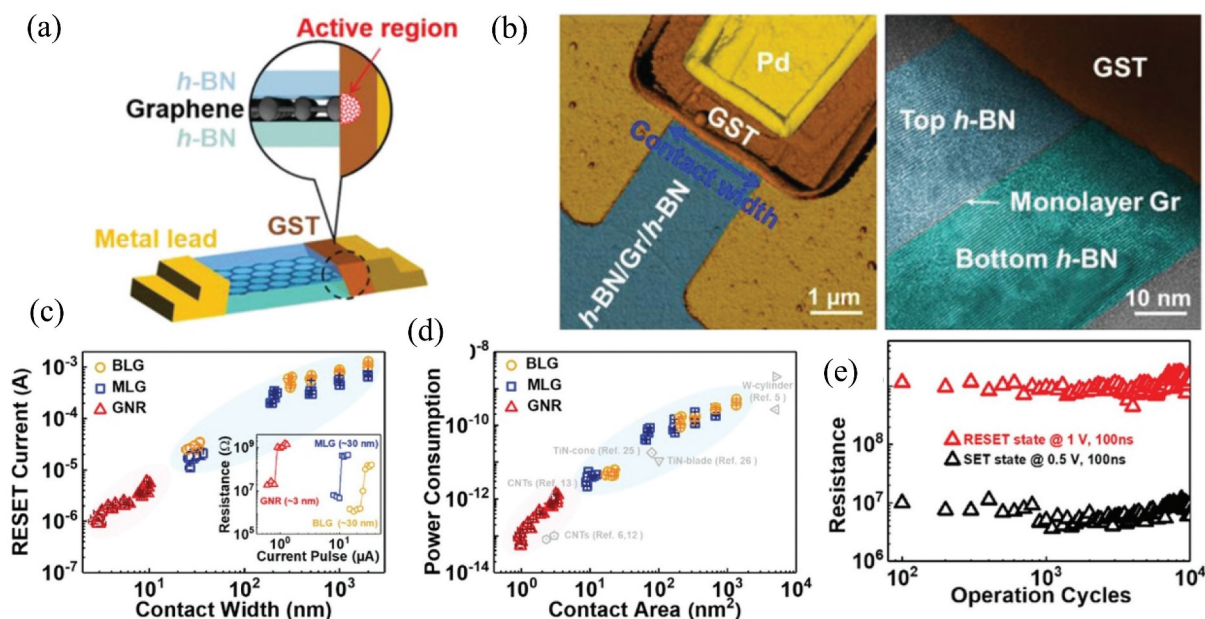


Figure 8. (a) Schematic of memory cell with graphene edge-contact. (b) Atomic force microscopy image of memory cell. (c) RESET current versus edge-contact width in memory cells. (d) Power consumption as a function of contact area. (e) Cycle endurance of memory cell. Reproduced by permission from [39], copyright [2022, Wiley].

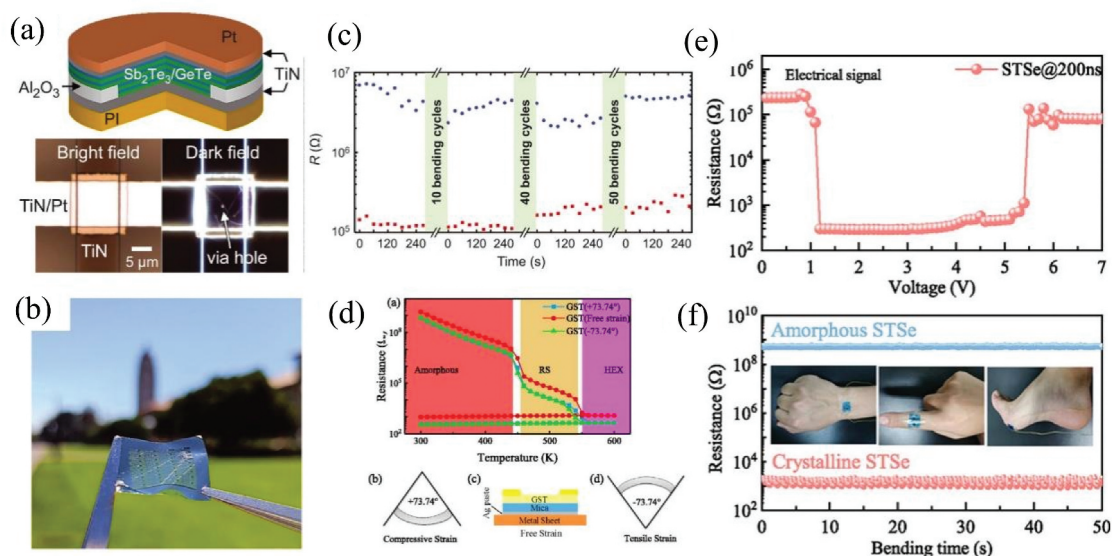


Figure 9. (a) Schematic and optical images of fabricated devices. (b) Photograph of flexible substrates with memory devices. Reproduced by permission from [40], copyright [2021, AAAS] (c) Resistance with cyclic bending. (d) Temperature dependence of resistance of amorphous films. Reproduced by permission from [41], copyright [2020, AIP] (e) Cell resistances measured as a function of the voltage pulse. (f) Variations in device resistance as a function of time. Reproduced by permission from [42], copyright [2022, ACS].

retention of over 100 h, demonstrating its excellent operational reliability. The combination of phase change and mechanical capabilities of these devices facilitates numerous applications for the flexible electronics that are under development. These flexible phase change materials and phase change memory related results guide the way in data storage in flexible IoT electronics, and open their application on flexible chalcogenide-based memory devices and wearable device application.

Uncovering the atomic dynamics of bonding and time evolution in functional materials with sophisticated lattice structures allows to update the rich physics involved and contributes to the manipulation of material properties on demand. Recent studies have proposed that instantaneous excitation of electrons allows cutting energy dissipation by introducing direct solid-solid amorphization that bypasses the molten state. Matsubara *et al.* presented a model for the rattling of GeTe and Ge₂Sb₂Te₅ crystals at photon energies of about

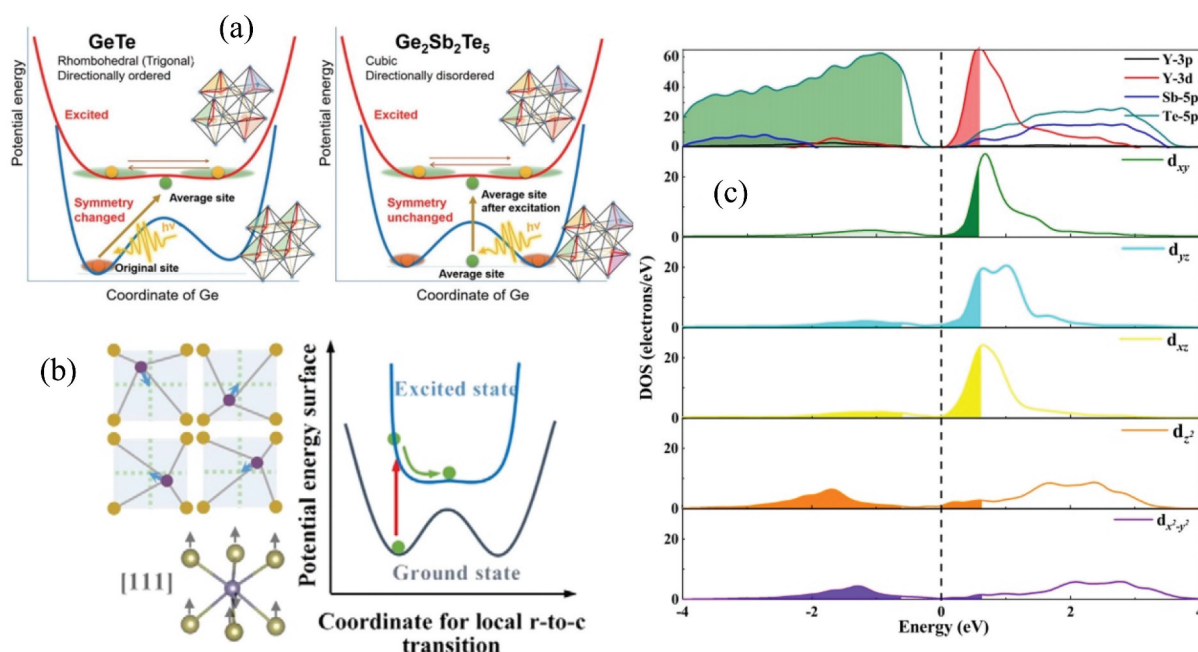


Figure 10. (a) Schematic diagrams of the instantaneous structural transitions of GeTe and Ge₂Sb₂Te₅. Reproduced by permission from [43], copyright [2016, APS] (b) Two-dimensional square mesh representing the suppression of local aberrations in the random orientation between the unit cells. Reproduced by permission from [44], copyright [2022, APS] (c) Partial density of states for the orbital decomposition of the Y-Sb-Te alloy including total PDOS and decomposition of d states. Reproduced by permission from [45], copyright [2022, APS].

1.55 eV, where Te remains in their original positions while Ge wobbles between six equivalents rhombohedral (r) phases at off-center positions because of excitation [43]. As shown in Figure 10(a), the rhombohedral GeTe lattice tends to transform into a cubic lattice via the rocking motion of Ge. On the other hand, since the rock salt Ge₂Sb₂Te₅ crystal has a random Peierls distortion, it is seen by X-rays to behave as a cubic crystal with its Ge atoms located at the average (central) position. Qi *et al.* focused on the sub-picosecond suppression of ultrafast electron X-rays in the average localized motif of rock salt Ge₂Sb₂Te₅ [44], in which ultrafast rhombic to cubic geometries can be seen by coherent phonon excitation quantified in terms of bond length dynamics, as shown in Figure 10(b). Chen *et al.* proposed photoinduced Y-Sb-Te undergoes an inhomogeneous and local ultrafast disordering in which all the degrees of freedom are excited simultaneously [45]. As shown in Figure 10(c), according to the dipole selection rule, the transition probability relies on the geometry of the orbitals, the results show that the Y-centered motif keeps not only its pinned effect when an intense laser is employed, which also comprises the electron-selective population behavior of the undiscovered Y-d_{t_{2g}} orbitals. Speaking of the above photoexcitation events, the photoinduced PCM community uncovers a hopping of the potential energy surface landscape, i.e. a transition from a multi-energy valley to a single-energy one. The dynamics serves as a prerequisite for phase transitions in favor of atoms overcoming the potential barriers, besides, the electronic response of the local structural motifs as well as electron-

phonon coupling allow to pursue the manipulation of the lattice dynamics.

The phase change materials radio frequency switches (PCRFS) relies on the phase change material to store '0' or '1' by the reversible structural transition between the crystalline state (semiconductor characteristics, low-resistance state, LRS) and amorphous state (metal characteristics, high-resistance state, HRS), thus realizing the 'on' and 'off' of RF switches with electrical signals turn-on and turn-off. The change value of resistivity between the amorphous state and the crystalline state can be capable of 4 ~ 5 orders of magnitude. Generally, energy pulse can be used to make the phase change material repeatedly transform between two states. According to the requirements of RF circuits, the on-state resistance of phase change materials can be reduced by adjusting properties and geometric structure of phase change material for the sake of low insertion loss in the open state. Therefore, the controllable and selectable signals can be realized by integrating PCRFS into RF circuits. The research of PCRFS began in 2008, since IBM designed a four-terminal switch topology using Ge₂Sb₂Te₅ thin film material [46]. A fabricated single-pole single-throw (SPST) phase change RF switch is exhibited in Figure 11(a). The 'on' and 'off' states of RF switch can be realized by voltage control of micro-heater (typically W) under the PCM. For biasing the monolithic RF phase change material switches, the applied actuation voltage pulses, measured current, measured temperature and measured resistance are

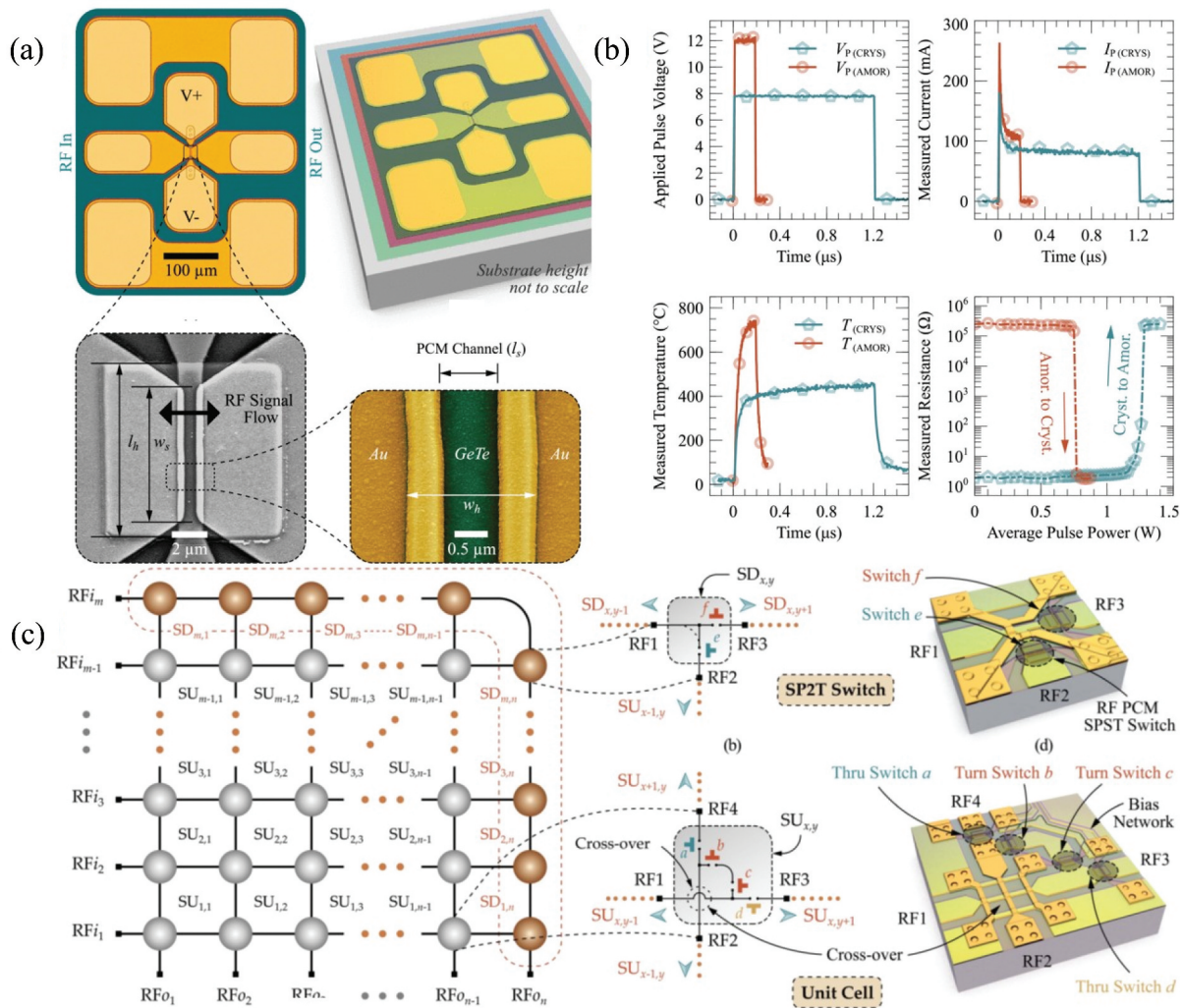


Figure 11. (a) a fabricated single-pole single-throw (SPST) phase change RF switch with a zoom-out view of the phase change materials channel. (b) a nonvolatile phase change between crystalline and amorphous states with applied voltage, measured current, measured temperature and measured resistance, respectively. Reproduced by permission from [46], copyright [2021, IEEE] (c) a scalable $m \times n$ matrix architecture consisting of switch unit cells and single-pole double-throw (SP2T) cells. Reproduced by permission from [47], copyright [2021, IEEE].

depicts in Figure 11(b,c). The PCRFS exhibit a more than five orders of magnitude in resistance ratio, which offer at least one magnitude higher resistance ratio compared with semiconductor-based RF switches. In addition, Tejinder Singh et al presents millimeter-wave (mmWave) chalcogenide nonvolatile GeTe-based scalable switch matrices in a crossbar configuration [47,48]. The switch matrices provide a novel way in a wide range of applications, such as wireless communication and automated equipment testing applications.

Matrix-vector multiplication, which offers peak speed and bandwidth density for data transfer, may be performed analogically using integrated photonic networks. Nonvolatile PCMs, when included in integrated photonic devices, can endow on-chip optical computing with crucial programming. A multimode photonic computer core comprising a number of programmable mode converters based on PCM-comprising on-waveguide meta-surfaces was demonstrated by

Wu et al. [49] Figure 12(a-c) show the device and control systems as well as the measurement results. The waveguide spatial modes are precisely controlled by programmable converters, up to 64 levels in modal contrast. An optical convolutional neural network was used for imaging recognition, as shown in Figure 12(d). A highly accurate conventional optical convolutional neural network was used for processing and recognizing images. Boybat et al. created a thorough model based on PCM units and used simulations to demonstrate its application [50]. Figure 12(e,f) show the synapses based on PCM and the applications of multi-memristive synapses in neural networks. They also provide experimental results for the unsupervised learning of temporal correlations using a spiking neural network, comprising over a million PCM devices. The proposed architecture in this study are a significant method towards the realization of highly efficient, large-scale neural networks based on memristive devices.

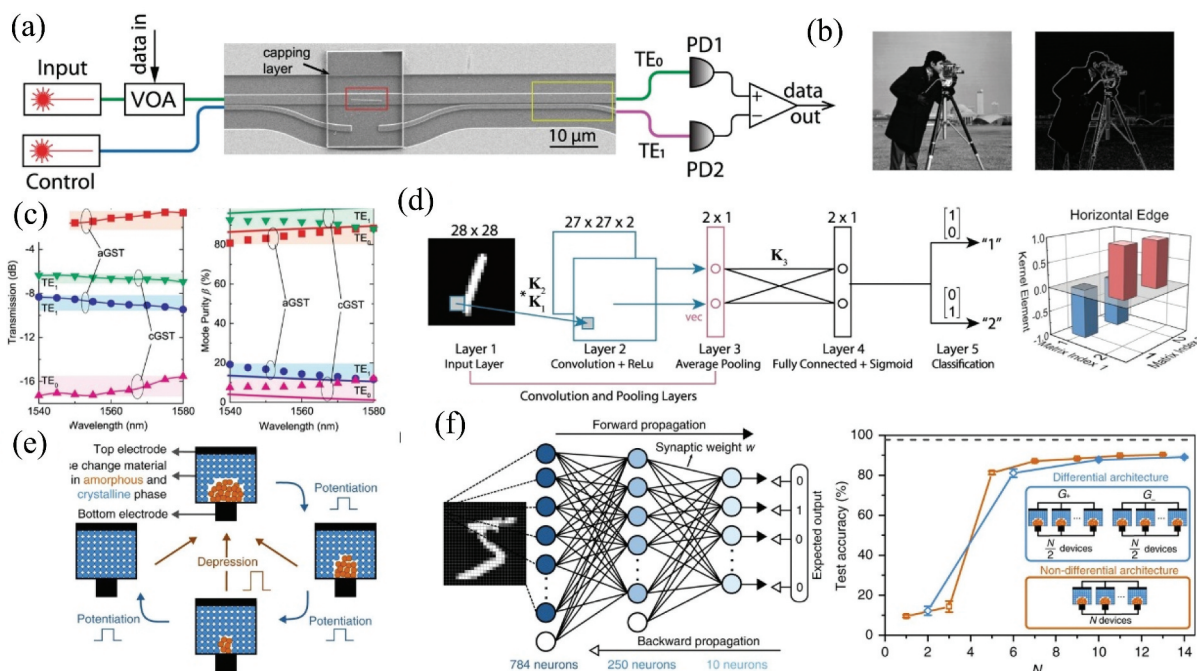


Figure 12. (a) and (b) Scanning electron microscopy image of the complete device, measurement results, and control schematics. (c) Transmission coefficient of the devices. (d) Optical convolutional neural network for imaging recognition. Reproduced by permission from [49], copyright [2021, Springer] (e) (f) Synapses based on PCM and applications of multi-memristive synapses in neural networks. Reproduced by permission from [50], copyright [2018, Springer].

The hardware implementation of neural networks is the focus of neuromorphic computing, and the device implementation of a single neuron and synapse has attracted significant research attention. Since the invention of memristors, studies on the imitation of synaptic

plasticity have been encouraging. The phase-change memristive synapse introduced by Sarwat et al. utilizes both the volatility of the field-effect modulation and the non-volatility of the phase configurations to enable adjustable plasticities [51]. Figure 13(a) shows the

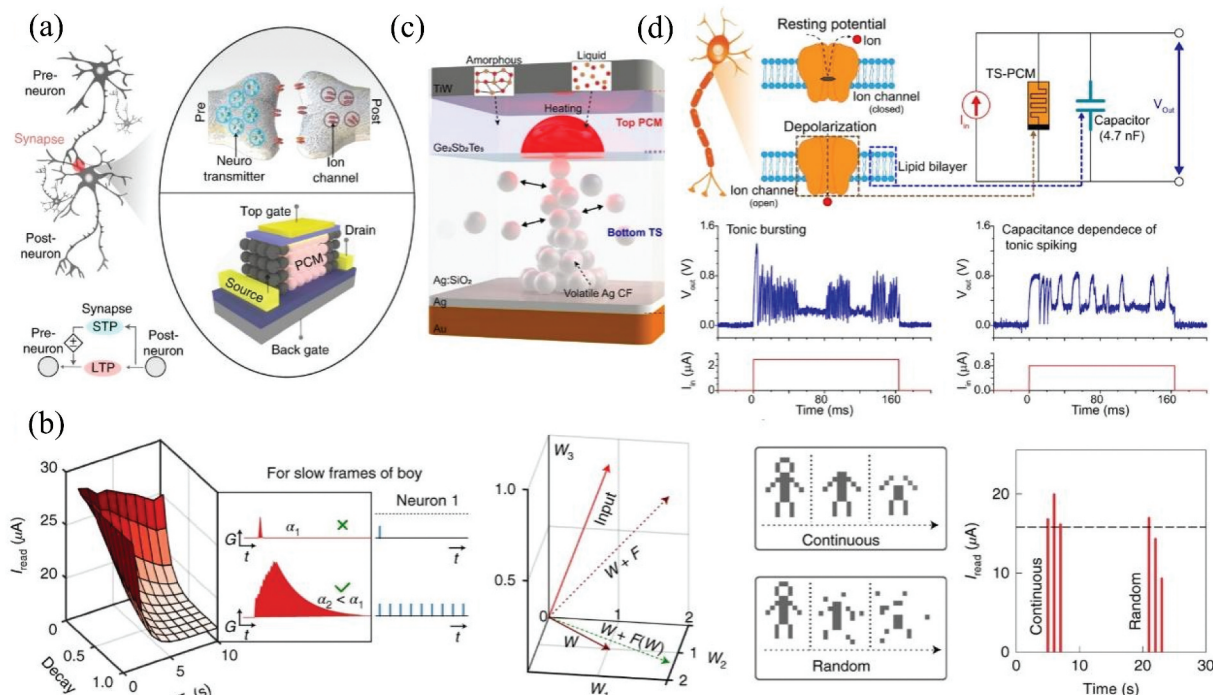


Figure 13. (a) Illustration of biological neurons. The enlarged view shows a biological synaptic junction (synapse) and its artificial emulation. (b) Tunable and weight-dependent short-term dynamics. Reproduced by permission from [51], copyright [2022, Springer] (c) Schematic of TS-PCM. (d) Emulation of spiking behavior and synaptic plasticity by TS-PCM. Reproduced by permission from [52], copyright [2022, Springer].

synaptic efficacy and phase-change memtransistors. To represent dynamic settings, these mixed-plasticity synapses can permit plasticity rules including short-term spike-timing-dependent plasticity. The tunable and weight-dependent short-term dynamics are shown in Figure 13(b). Additionally, the effectiveness of memtransistive synapses in realizing Hopfield neural network accelerators for tackling combinatorial optimization issues was demonstrated. A neurosynaptic device that simultaneously simulates synaptic and intrinsic plasticity in a single cell was reported by Sung et al. [52]. Figure 13(c) shows a schematic of TS-PCM composed of volatile TS and a nonvolatile PCM layer. Threshold switches and phase-change memories are combined in threshold switch-PCM (TS-PCM) devices. Figure 13(d) shows the emulation of spiking behavior and synaptic plasticity using TS-PCM. Based on the bottom threshold switch layer to simulate the modification of firing frequency in biological neurons, the neuronal intrinsic plasticity is demonstrated. Through the nonvolatile switching of the top phase change layer, synaptic plasticity is also facilitated. A single cell concurrently mimics intrinsic and synaptic plasticity to provide positive feedback between them. This work demonstrations clearly showcase the efficacy of PCM devices for neuromorphic computing. Overall, the rapid phase transitions together with the strong property contrast between crystalline and amorphous states make PCMs an ideal choice for future nanoelectronic and nanophotonic applications.

Summary

Although PCM has excellent prospects, challenges such as further reducing cost and power consumption, improving writability and storage density, and reducing resistance drift should be overcome to facilitate high-precision analog computing. Moreover, in the chip industry, it is believed that Moore's Law is close to failure. With an increasing number of transistors in the chip, the problem of electronic energy leakage and heat dissipation has gradually been increasing, and significant difficulties concerning device miniaturization and large-scale array integration are being faced.

In the application of neural morphology computing system, compared with central processing unit, PCM uses vector-matrix multiplication to accelerate artificial neural network, and adopts large-scale parallel computing, which significantly facilitates fault tolerance and computing speed. Moreover, its power consumption is also significantly lower than that of graphics processing unit. In addition, in the future, a combination of hardware and software is required to realize the construction mode of artificial neural networks. In terms of hardware, it challenging to study the core PCMs and the optimal device structure.

Herein, the principle of PCMs is introduced, the corresponding relationship between the application requirements of devices and the performance of PCM is reviewed, and the research status and application prospects of phase-change memories are elucidated. Determining ways to develop PCMs in the form of devices for data storage applications, and further expanding them to computing applications, from simple logic operations to complex neural morphology computing should be the direction for future research. Based on these factors, we firmly believe that PCM will be more widely recognized in the upcoming years.

Disclosure statement

No potential conflict of interest was reported by the author(s).

Funding

This work was financially supported by the National Natural Science Foundation of China [Grant Nos. 62090015, 62374043].

Notes on contributors



Kai Jiang is a professor at School of Arts and Sciences, Shanghai Dianji University since 2023. He received his B.S. from Yantai University in 2009 and Ph.D. from East China Normal University in 2014. Afterward, he worked as a postdoctoral fellow in Shanghai Institute of Technical Physics Chinese Academy of Sciences (2014–2016) and an associate professor in East China Normal University (2017–2022). His scientific interest is in situ condensed matter spectroscopy under extreme conditions.



Shubing Li is a Ph. D. candidate at the Department of Physics, East China Normal University since 2020. He received his B.S. and M.S. in 2017 and 2020 from Shandong University and Nanjing University of Aeronautics and Astronautics, respectively. His major research focus on phase change materials based memories and RF switches.



Fangfang Chen has been a lecturer at School of Arts and Sciences, Shanghai Dianji University, China, since 2021. She received her B.S and M.S. in 2013 and 2016 from Changshu Institute of Technology and Zhejiang Normal University, respectively. In 2020, she obtained a Ph. D. in East China Normal University. Her current research interests include the electrical properties of phase change materials and two-dimensional materials-based electronics.



Liping Zhu is an engineer at State Key Laboratory of Surface Physics and Institute for Nanoelectronic Devices and Quantum Computing, Department of Physics, Fudan University, Shanghai, China. She received her B.S. and Ph.D. in 2009 and 2014 in Microelectronics and Solid-State Electronics from East China Normal University. Her current research interests include semiconductor material physics and device technology.



Wenwu Li received his Ph.D. degree in Microelectronics and Solid-State Electronics from East China Normal University, China in 2012. From 2012 to 2014, he worked as a postdoctoral researcher at the National Institute for Materials Science (Japan) and China Southern Power Grid Corporation. From 2014 to 2021, he worked as a full professor at East China Normal University. Since August 2021, he is serving as a full professor at Fudan University, China. His research field focuses on microelectronic and optoelectronic devices. For more information: (<https://ioe.fudan.edu.cn/55/ec/c34075a415212/page.htm>)

ORCID

Kai Jiang  <http://orcid.org/0000-0002-5117-6941>

Wenwu Li  <http://orcid.org/0000-0002-9307-1566>

References

- [1] Sarwat S, Philip T, Chen C, et al. Projected mushroom type phase-change memory. *Adv Func Mater.* 2021;31:2106547. doi: [10.1002/adfm.202106547](https://doi.org/10.1002/adfm.202106547)
- [2] Chen X, Xue Y, Sun Y, et al. Neuromorphic photonic memory devices using ultrafast, non-volatile phase-materials. *Adv Mater.* 2022;2203909:1–7. doi: [10.1002/adma.202203909](https://doi.org/10.1002/adma.202203909)
- [3] Zhou X, Kalikka J, Ji X, et al. Phase-change memory materials by design: a strain engineering approach. *Adv Mater.* 2016;28(15):3007–3016. doi: [10.1002/adma.201505865](https://doi.org/10.1002/adma.201505865)
- [4] Aryana K, Gaskins J, Nag J, et al. Interface controlled thermal resistance of ultra-thin chalcogenide-based phase change memory devices. *Nat Commun.* 2021;12:774. doi: [10.1038/s41467-020-20661-8](https://doi.org/10.1038/s41467-020-20661-8)
- [5] Liu Y, Li X, Zheng H, et al. High-throughput screening for phase-change memory materials. *Adv Funct Mater.* 2021;31(21):2009803. doi: [10.1002/adfm.202009803](https://doi.org/10.1002/adfm.202009803)
- [6] Xie Y, Kim W, Kim Y, et al. Self-healing of a confined change memory device with a metallic surfactant layer. *Adv Mater.* 2018;30:1705587. doi: [10.1002/adma.201705587](https://doi.org/10.1002/adma.201705587)
- [7] Sarwat S, Gallo M, Bruce R, et al. Mechanism and impact of bipolar current voltage asymmetry in computational phase-change memory. *Adv Mater.* 2022;2201238:1–9. doi: [10.1002/adma.202201238](https://doi.org/10.1002/adma.202201238)
- [8] Kersting B, Sarwat S, Gallo M, et al. Measurement of onset of structural relaxation in melt-quenched phase change materials. *Adv Func Mater.* 2021;31:2104422. doi: [10.1002/adfm.202104422](https://doi.org/10.1002/adfm.202104422)
- [9] Lu Y, Li X, Yan B, et al. In-memory realization of eligibility traces based on conductance drift of phase change memory for energy-efficient reinforcement learning. *Adv Mater.* 2022;34:2107811. doi: [10.1002/adma.202107811](https://doi.org/10.1002/adma.202107811)
- [10] Kim D, Lee H, You B, et al. Flexible crossbar-structured phased change memory array via mo-based interfacial physical lift-off. *Adv Funct Mater.* 2019;29:1806338. doi: [10.1002/adfm.201806338](https://doi.org/10.1002/adfm.201806338)
- [11] Pries J, Weber H, Benke-Jacob J, et al. Fragile-to-strong transition in phase-change material Ge₃Sb₆Te₅. *Adv Funct Mater.* 2022;32:2202714. doi: [10.1002/adfm.202202714](https://doi.org/10.1002/adfm.202202714)
- [12] Khan A, Wu X, Perez C, et al. Unveiling the effect of superlattice interfaces and intermixing on phase change memory performance. *Nano Lett.* 2022;22:6285–6297. doi: [10.1021/acs.nanolett.2c01869](https://doi.org/10.1021/acs.nanolett.2c01869)
- [13] Joshi V, Gallo M, Haefeli S, et al. Accurate deep neural network inference using computational phase-change memory. *Nat Commun.* 2020;11:2437. doi: [10.1038/s41467-020-16108-9](https://doi.org/10.1038/s41467-020-16108-9)
- [14] Gui H, Yang T, Li L, et al. Temperature sensitive anti-inflammatory organohydrogels containing janus particle stabilized phase-change microinclusions. *ACS Nano.* 2022;16:9859–9870. doi: [10.1021/acsnano.2c03940](https://doi.org/10.1021/acsnano.2c03940)
- [15] Pries J, Stenz C, Schäfer L, et al. Resistance drift convergence and inversion in amorphous phase change materials. *Adv Funct Mater.* 2022;32:2207194. doi: [10.1002/adfm.202207194](https://doi.org/10.1002/adfm.202207194)
- [16] Sarwat S, Kersting B, Moraitis T, et al. Phase-change memtransistive synapses for mixed-plasticity neural computations. *Nat Nanotech.* 2022;17:507–513. doi: [10.1038/s41565-022-01095-3](https://doi.org/10.1038/s41565-022-01095-3)
- [17] Minh D, Nguyen L, Trinh C, et al. Low-dimensional single-cation formamidinium lead halide perovskites (Fam+2PbmBr_{3m+2}): from synthesis to rewritable phase-change memory film. *Adv Funct Mater.* 2021;31(17):2011093. doi: [10.1002/adfm.202011093](https://doi.org/10.1002/adfm.202011093)
- [18] Xu Y, Wang X, Zhang W, et al. Materials screening for disorder-controlled chalcogenide crystals for phase-change memory applications. *Adv Mater.* 2021;33(9):2006221. doi: [10.1002/adma.202006221](https://doi.org/10.1002/adma.202006221)
- [19] Adinolsi V, Cheng L, Laudato M, et al. Composition-controlled atomic layer deposition of phase-change memories and ovonic threshold switches with high performance. *ACS Nano.* 2019;13:10440–10447. doi: [10.1021/acsnano.9b04233](https://doi.org/10.1021/acsnano.9b04233)
- [20] Yoo C, Jeon J, Yoon S, et al. Atomic layer deposition of Sb₂Te₃/GeTe superlattice film and its melt-quenching-free phase-transition mechanism for phase-change memory. *Adv Mater.* 2022;34:2207143. doi: [10.1002/adma.202207143](https://doi.org/10.1002/adma.202207143)
- [21] Modi G, Stach E, Agarwal R. Low-power switching through disorder and carrier localization in bismuth-doped germanium telluride phase change memory nanowires. *ACS Nano.* 2020;14(2):2162–2171. doi: [10.1021/acsnano.9b08986](https://doi.org/10.1021/acsnano.9b08986)
- [22] Farmalidis N, Youngblood N, Li X, et al. Plasmonic nanogap enhanced phase-change devices with dual electrical-optical functionality. *Sci Adv.* 2019;5:eaaw2687. doi: [10.1126/sciadv.aaw2687](https://doi.org/10.1126/sciadv.aaw2687)
- [23] Ríos C, Stegmaier M, Hosseini P, et al. Integrated all-photonic non-volatile multi-level memory. *Nat*

- Photonics. 2015;9:725–732. doi: 10.1038/nphoton.2015.182
- [24] Le Gallo M, Sebastian A. An overview of phase-change memory device physics. *J Phys D App Phys*. 2020;53:213002. doi: 10.1088/1361-6463/ab7794
- [25] Rao F, Ding KY, Zhou YX, et al. Reducing the stochasticity of crystal nucleation to enable subnanosecond memory writing. *Science*. 2017;358:1423–1427. doi: 10.1126/science.aao3212
- [26] Zewdie GM, Zhou Y, Sun L, et al. Chemical design principles for cache-type Sc–Sb–Te phase-change memory materials. *Chem Mater*. 2019;31(11):4008–4015. doi: 10.1021/acs.chemmater.9b00510
- [27] Yang Z, Li B, Wang JJ, et al. Designing conductive-bridge phase-change memory to enable ultralow programming power. *Adv Sci*. 2022;9:e2103478. doi: 10.1002/advs.202103478
- [28] Xu Y, Zhou Y, Wang XD, et al. Unraveling crystallization mechanisms and electronic structure of phase-change materials by large-scale ab initio simulations. *Adv Mater*. 2022;34:e2109139. doi: 10.1002/adma.202109139
- [29] Zalden P, Quirin F, Schumacher M, et al. Femtosecond x-ray diffraction reveals a liquid-liquid phase transition in phase-change materials. *Science*. 2019;364:1062–1067. doi: 10.1126/science.aaw1773
- [30] Xu Z, Park K, Schneeloch J, et al. Metal-insulator transition and doping-induced phase change in $\text{Ge}_2\text{Sb}_2\text{Se}_{5x}\text{Te}_{5-5x}$. *Appl Phys Lett*. 2020;117:193503. doi: 10.1063/5.0030956
- [31] Shuang Y, Hatayama S, Saito Y, et al. Evolution of the local structure surrounding nitrogen atoms upon the amorphous to crystalline phase transition in nitrogen-doped $\text{Cr}_2\text{Ge}_2\text{Te}_6$ phase-change material. *Appl Surface Sci*. 2021;556:149760. doi: 10.1016/j.apsusc.2021.149760
- [32] Cheng Y, Yang Q, Wang J, et al. Highly tunable β -relaxation enables the tailoring of crystallization in phase-change materials. *Nat Commun*. 2022;13:7352. doi: 10.1038/s41467-022-35005-x
- [33] Delaney M, Zeimpekis L, Lawson D, et al. A new family of ultralow loss reversible phase-change materials for photonic integrated circuits: Sb_2S_3 and Sb_2Se_3 . *Adv Funct Mater*. 2020;30:2002447. doi: 10.1002/adfm.202002447
- [34] Ding K, Wang J, Zhou Y, et al. Phase-change heterostructure enables ultralow noise and drift for memory operation. *Science*. 2019;366(6462):210–215. doi: 10.1126/science.aay0291
- [35] Shen J, Jia S, Shi M, et al. Elemental electrical switch enabling phase segregation free operation. *Science*. 2021;374:1390–1394. doi: 10.1126/science.abi6332
- [36] Cheng Y, Cai D, Zheng Y, et al. Microscopic mechanism of carbon-dopant manipulating device performance in CGeSbTe -based phase change random access memory. *ACS Appl Mater Interfaces*. 2020;12(20):23051–23059. doi: 10.1021/acsami.0c02507
- [37] Liu B, Li K, Liu W, et al. Multi-level phase-change memory with ultralow power consumption and resistance drift. *Sci Bull*. 2021;66:2217–2224. doi: 10.1016/j.scib.2021.07.018
- [38] Liu B, Liu W, Li Z, et al. Y-doped Sb_2Te_3 phase-change materials: toward a universal memory. *ACS Appl Mater Interfaces*. 2020;12(18):20672–20679. doi: 10.1021/acsami.0c03027
- [39] Wang X, Song S, Wang H, et al. Minimizing the programming power of phase change memory by using graphene nanoribbon edge-contact. *Adv Sci*. 2022;9:2202222. doi: 10.1002/advs.202202222
- [40] Khan A, Daus A, Islam R, et al. Ultralow-switching current density multilevel phase-change memory on a flexible substrate. *Science*. 2021;373:1243–1247. doi: 10.1126/science.abj1261
- [41] Li M, Xie M, Ji H, et al. PLD-derived $\text{Ge}_2\text{Sb}_2\text{Te}_5$ phase-change films with extreme bending stability for flexible device applications. *Appl Phys Lett*. 2020;116:162102. doi: 10.1063/5.0001348
- [42] Li S, Li M, Chen L, et al. Ultra-stable, enduring, and flexible $\text{Sb}_2\text{Te}_x\text{Se}_{3-x}$ phase change devices for memory application and wearable electronics. *ACS Appl Mater Interfaces*. 2022;14:45600–45610. doi: 10.1021/acsami.2c13792
- [43] Matsubara E, Okada S, Ichitsubo T, et al. Initial atomic motion immediately following femtosecond-laser excitation in phase-change materials. *Phys Rev Lett*. 2016;117(13):135501. doi: 10.1103/PhysRevLett.117.135501
- [44] Qi Y, Chen N, Vasileiadis T, et al. Photoinduced ultrafast transition of the local correlated structure in chalcogenide phase-change materials. *Phys Rev Lett*. 2022;129(13):135701. doi: 10.1103/PhysRevLett.129.135701
- [45] Chen L, Cui A, Li M, et al. Optical excitation-induced ultrafast amorphization in the Y–Sb–Te alloy system: insights from real-time time-dependent DFT with molecular dynamics calculations. *Phys Rev B*. 2022;106(21):214110. doi: 10.1103/PhysRevB.106.214110
- [46] Chen KN, Krusin-Elbaum L, Newns DM, et al. Programmable via using indirectly heated phase change switch for reconfigurable logic applications. *IEEE Electr Device L*. 2008;29:131–133. doi: 10.1109/LED.2007.912016
- [47] Singh T, Mansour RR. Experimental investigation of performance, reliability, and cycle endurance of non-volatile DC–67 GHz phase-change RF switches. *IEEE T Microw Theory*. 2021;69:4697–4710. doi: 10.1109/TMTT.2021.3105413
- [48] Singh T, Mansour RR. Ultra-compact phase-change GeTe -based scalable mmWave latching crossbar switch matrices. *IEEE T Microw Theory*. 2021;70:938–949. doi: 10.1109/TMTT.2021.3128589
- [49] Wu C, Yu H, Lee S, et al. Programmable phase-change metasurfaces on waveguides for multimode photonic convolutional neural network. *Nat Commun*. 2021;12:96. doi: 10.1038/s41467-020-20365-z
- [50] Boybat I, Gallo M, Nandakumar S, et al. Neuromorphic computing with multi-memristive synapses. *Nat Commun*. 2018;9:2514. doi: 10.1038/s41467-018-04933-y
- [51] Sarwat S, Kersting B, Moraitis T, et al. Phase-change memtransistive synapses for mixed-plasticity neural computations. *Nat Nanotech*. 2022;17:507–573. doi: 10.1038/s41565-022-01095-3
- [52] Sung S, Kim T, Shin H. Simultaneous emulation of synaptic and intrinsic plasticity using a memristive synapse. *Nat Commun*. 2022;13:2811. doi: 10.1038/s41467-022-30432-2